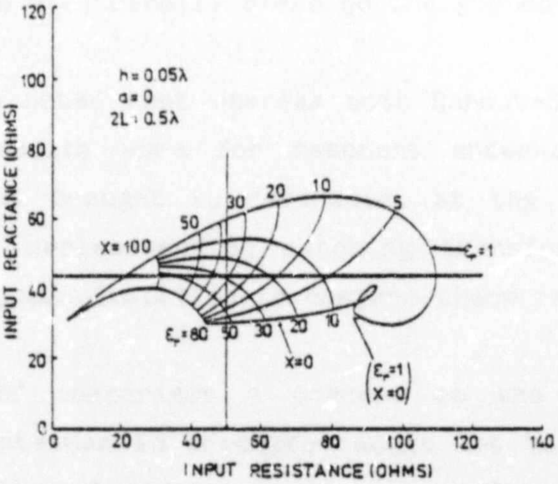

Figure 6.11 : Measured values for the case where antenna height is 0,054λ above imperfect earth.

At 1,25m R_1 = 66,8Ω and X_1 = 56,9Ω. From Fig. 6.10 we read ε_r = 28 and then calculate $\sigma = 1,14 \times 10^{-2}$ Sm^{-1}. Using the measured data from 3 m, R_1 = 49,8Ω and X_1 = 44,2Ω and from Fig. 6.11 we obtain almost exactly the values found above, at L = 1,25 m, for σ and ε_r. Both values are markedly higher than those quoted earlier for rural ground, but Sweeting and Davis (1980), working with radial metallic ground systems for short monopole antennas at HF, measured values of ε_r between 30 and 34, by two independent methods. Their test site was similar in many respects to that used here. In addition Vice (1954) measured σ in the range from 4 to $6,5 \times 10^{-3}$ Sm^{-1}, in the same geographical area, at medium frequencies. At higher frequencies σ would increase.

The effects of the ground on the performance of HF antennas at low heights is a vast subject in its own right and somewhat beyond the intended purpose of this work. There is however a vast amount of literature on the topic which shows unequivocally that the complex nature of the ground's electrical characteristics and their variability with geographical location can be expected to affect antennas which are electrically close to the ground-air interface.

It should also be noted that whereas both Rahmat-Samii et al and Burke et al's results were for resonant antennas the antenna discussed here was brought to resonance, at the frequencies in question, by the series-section matching transformer, L_2. It would therefore appear justified to compare these results.

Finally by way of comparison a comment on the efficiency of halfwave dipole antennas in freespace would not be out of place. Fitz-Gerrell (1965) analyzed this well-used configuration in order to show how valid the usual assumption of 100 per cent efficiency was, given different conductor diameters and material conductivity. He produced the following useful equation for efficiency:

$$\eta = \frac{100}{1 + \frac{\lambda}{8\pi a}\sqrt{\frac{\omega\mu}{2\sigma}} \Big/ 73{,}12} \quad \% \qquad (6.3)$$

where a is conductor radius.

For example, an antenna of 4 mm diameter copper has an efficiency of 99,33 per cent whereas for one of 4 mm steel it is 96,5 per cent. Any further decrease in efficiency would then be due to ground- or other environmental losses.

6.1.3 The effect on system performance of increasing L_1

We now turn our attention to the original design frequencies of the antenna: those in the 1:2:2,5:3,5:4 f_N series and the results displayed in Fig. 6.3. As was noted previously the optimum frequencies were slightly higher than designed and so L_1 was then increased, somewhat arbitrarily, from 26,51 m (physical) to 27,51m. L_2 was unchanged at 12,2 m (physical). Again $Z_3|\underline{\emptyset_3}$ was measured and the results, normalized with respect to $Z_4 = 50\Omega$, are shown in Fig. 6.12.

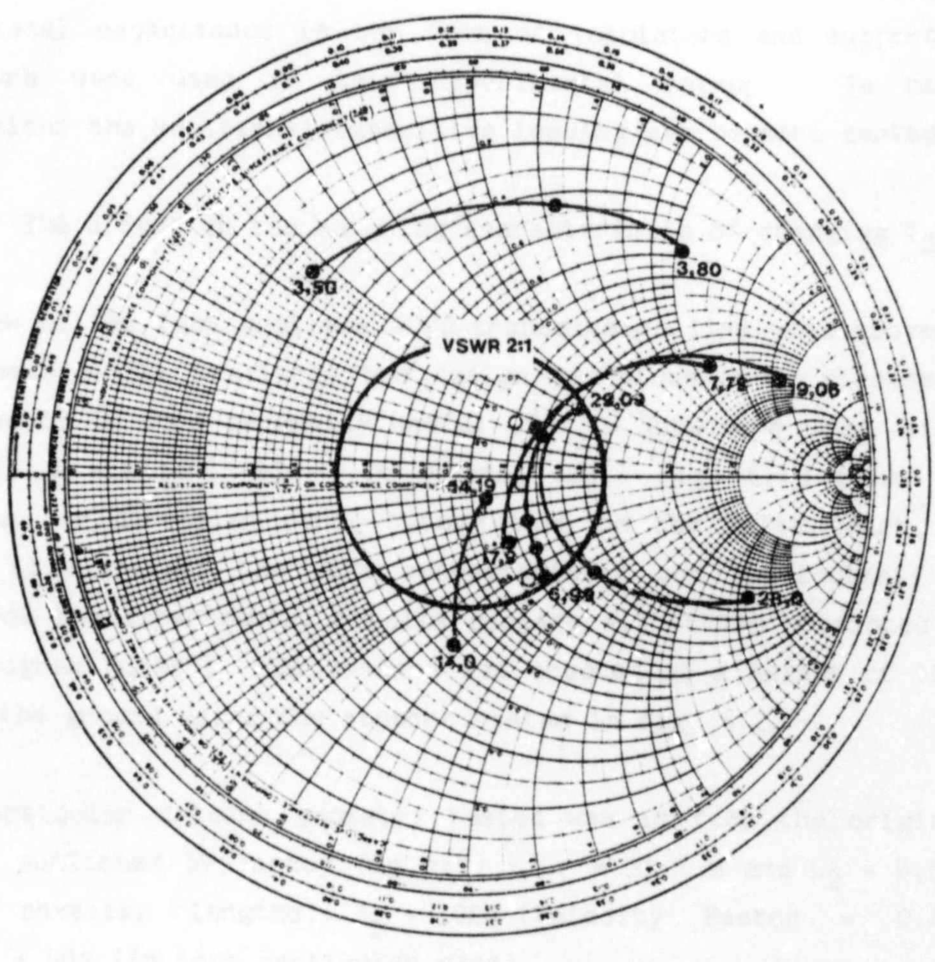

Figure 6.12 : Measured values of Z_3 normalized with respect to Z_4 for L_1 = 27,51 m; L_2 = 12,2 m; $Z_2 = 400\Omega$ and $Z_4 = 50\Omega$. (Note that the 24 MHz band is shown as (o) from 24,69 to 24,92 MHz). Antenna height = 12m

Again two points are noteworthy. The first is that no match occurs on the 3,5 MHz band; in fact the impedance occupies almost the predicted freespace position on the chart, as was shown in Fig. 6.4. Second are the new results for the designed frequencies. These should be compared with those in Fig. 6.3. It will be noted that with L_1 now about 3,8 percent longer the antenna performs almost exactly as designed. The frequencies at which the loci of each of the impedance characteristics cross the real axis of the Smith Chart agree very closely with those predicted by the program "G5RV" and as listed in Table 6.1.

Less compensation for "end-effect" than the 5 per cent introduced would seem to be in order. (It should be noted that minimal additional capacitance in the form of insulators and supporting hardware were used in this experimental set-up. In other situations the additional capacitive loading may be more marked).

6.1.4 The effect on the matching characteristic of changing Z_2

In view of the fact that the 400Ω transmission line used above is not commercially available the design technique under discussion here would be more generally useful if Z_2 = 300Ω were used, since this is a standard value, in general use. Fig. 6.13 shows the results, in cartesian form, rather than on the Smith Chart, in order to highlight the VSWR characteristic and particularly to show how the experimental results compare with those predicted by the program "G5RV". The antenna was erected at a height of 10 m above the ground using the support syst - in Fig. 6.2.

The particular antenna geometry tes. d w in fact the original design published by Varney (op cit) : L_1 = 31,1 m and L_2 = 8,5 m (both physical lengths); Z_2 = 300Ω (Velocity Factor = 0,82) and Z_4 = 50Ω (in this particular case).

It will be noted that there is fair agreement between the measured and predicted results in the 3,7; 7,9 and 14,1 MHz bands and very good agreement in the 21 and 25 MHz bands. As noted earlier in criticism of the original Varney dimensions only 25 MHz actually exhibits a VSWR of less than the 2:1 criterion, hence from an operational point of view the antenna is not optimised. The form of the curves though does confirm once again the validity of the computer-based analytical technique. In the light of the findings in (6.1.2) the difference between the measured and predicted results on the lower three bands may be caused by the antenna coupling to the lossy ground. At 21 and 25 MHz it is 0,7 and 0,83λ above the interface respectively, which from Fig. 6.9 suggests that the driving point impedance Z_1 would be almost the free space value, whereas on the lower frequencies the height varies from 0,12λ to 0,47λ so changes in input resistance would occur.

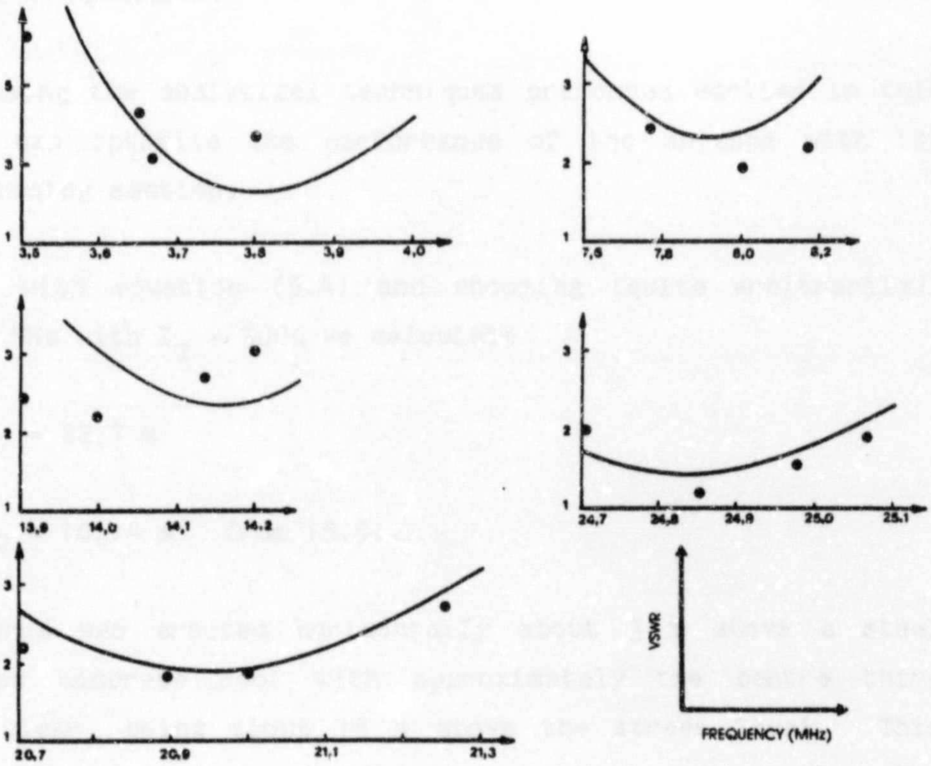

Figure 6.13 : Comparison of measured and predicted values of VSWR as a function of frequency for the original Varney design; (●) measured, (–) predicted

Examination of those frequencies in Fig. 6.13 at which the predicted VSWR is a minimum shows that they are related by the f_N series 1:2,09 : 3,77 : 5,6 : 6,6, if all bands including that around 3,7 MHz are considered. If, on the other hand, the 3,7 MHz band is ignored because of the marked ground coupling noted earlier, then the series is 1 : 1,8, : 2,68 : 3,16, with f_{min} of 7,9 MHz. This series should be compared with that for the first five frequencies on which a match occurs, shown in Table 5.6: viz 1 : 2,01 : 2,54 : 3,52 : 4,09. The differences are marked, leading us to conclude that the optimization procedure which changes L_1 and L_2, for given Z_2 and Z_4, will ultimately yield only a narrow range of combinations which provide a match on a maximum number of frequencies.

Now by using the analytical techniques presented earlier in this work we can optimise the performance of the antenna with the 300Ω matching section.

Starting with equation (5.4) and choosing (quite arbitrarily) f_{min} = 9 MHz with Z_2 = 300Ω we calculate

$$L_1 = 22,7 \text{ m}$$

and

$$L_2 = 10,14 \text{ m} \quad \text{from (5.5)}.$$

The antenna was erected horizontally about 3 m above a steel reinforced concrete roof with approximately the centre third hanging clear, being about 15 m above the street level. This installation is typical of many in an urban environment. The measured values of VSWR on all the bands on which an acceptable match of 2:1 or better occurred are shown in Fig. 6.14. Also shown are the predicted values of VSWR as a function of frequency for the antenna configuration yielding the best fit to the experimental data. The values which produced these results are:

$$L_1 = 22,0 \text{ m (electrical)}$$
$$L_2 = 9,95 \text{ m (electrical)}$$
$$Z_2 = 360\Omega$$
$$Z_4 = 50\Omega$$

In general the agreement between the measured results and those fitted is good. Certainly the 18 and 23 MHz bands confirm this while the 9 MHz band shows the same form with only a vertical displacement due possibly to its close coupling to its immediate surroundings, as suggested previously in relation to Fig. 6.13. The two highest frequency bands again exhibit the same form but there is evidence at 32 MHz, confirmed at 38 MHz, of a displacement

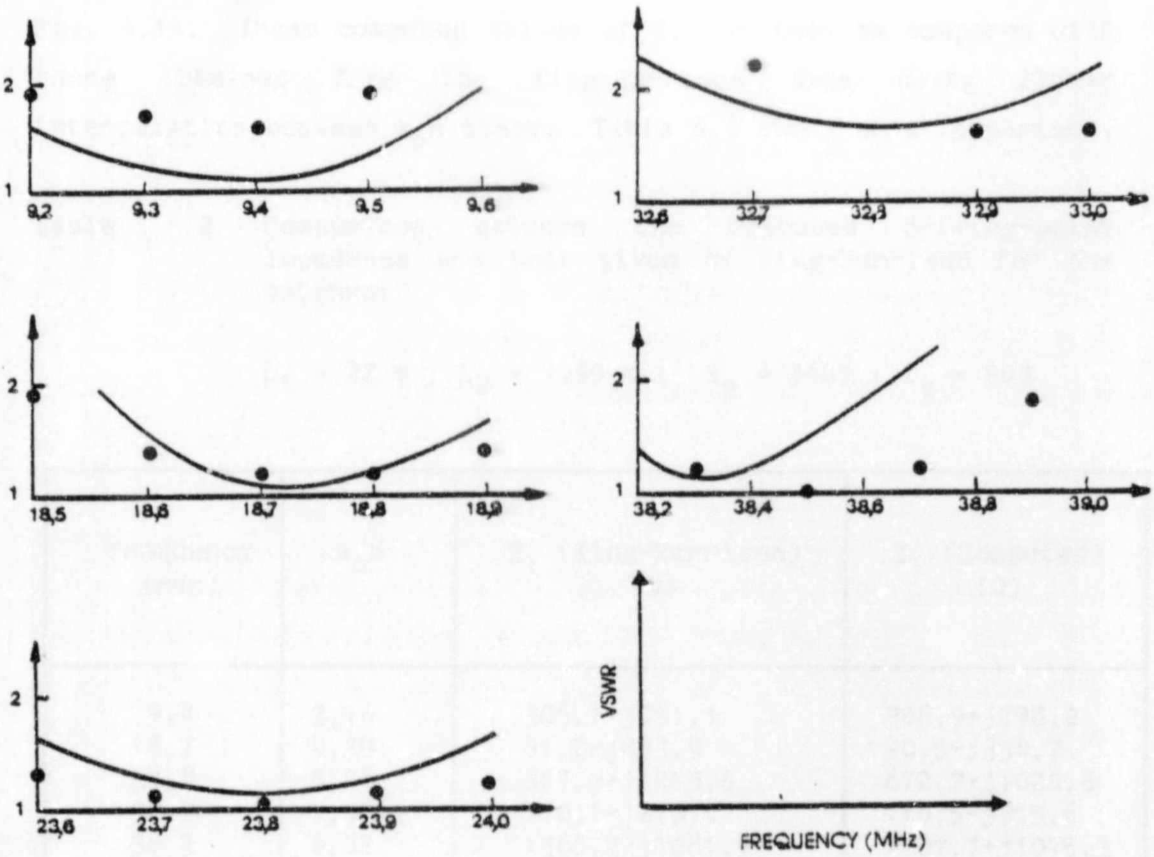

Figure 6.14 : The measured and "best fit" predicted results for an optimised antenna configuration; (●) measured, (—) predicted

of the measured results to the right. The error at 38 MHz between predicted and measured frequencies at which the minimum VSWR occurs is only 0,5 per cent however, which would seem to be tolerable. Why the characteristic impedance of Z_2 was 360Ω as opposed to the 300Ω used in the experimental antenna is not quite clear at this stage. One could speculate that the driving-point impedance, Z_1, is not that given by the freespace, King-Harrison data, but is some other value affected by the proximity of the building beneath the antenna. A value of Z_2 of 360Ω rather than 300Ω might then have been necessary to yield the required match. This impedance will be examined again later in this work.

It is however a simple matter, by using the analytical software developed for this study, to determine Z_1 from the calculated values of Z_3 which were used to produce the predicted VSWRs in Fig. 6.14. These computed values of Z_1 can then be compared with those obtained from the King-Harrison data using linear interpolation between k_oh steps. Table 6.2 shows this comparison.

Table 6.2 Comparison between the computed driving-point impedance and that given by King-Harrison for the antenna:

$$L_1 = 22\text{ m} ;\ L_2 = 9{,}95\text{ m} ;\ Z_2 = 360\Omega ;\ Z_4 = 50\Omega$$

Frequency (MHz)	k_oh	Z_1 (King-Harrison) (Ω)	Z_1 (Computed) (Ω)
9,4	2,16	305,1+j791,1	306,9+j798,2
18,7	4,30	91,2-j343,9	90,5-j334,7
23,8	5,48	667,3+j1015,6	672,7+j1020,8
32,8	7,55	110,1-j218,9	110,5-j215,6
38,3	8,82	1366,2+j1081,9	1407,7+j1075,3

The resistive values from 9,4 to 32,8 MHz differ by less than 1 per cent and by 3 per cent at 38,3 MHz while the reactive components never differ by more than 3 per cent. These results are significant and we must therefore conclude that any environmental effect at these frequencies and heights above "ground" are small. The freespace data can therefore be used with confidence.

So far it has been implicitly assumed that the matching section, Z_2, used in these measurements had a characteristic impedance of 300Ω. In view of the 360Ω predicted, a piece of this line was measured over the HF band to determine its actual characteristic impedance. The results are shown in Appendix J, where a value of 355Ω is far more representative of the true Z_2. That finding now lends considerable credibility to the predicted VSWR curves of Fig. 6.14.

6.1.5 The use of a single mast mount and its effect on antenna performance

As stated earlier an inverted vee configuration using a single mast to support the feedpoint of the antenna would have decided advantages over its two-mast counterpart, particularly in temporary or tactical situations. The geometry was shown in Fig. 6.1. The apex angle, Θ, is of prime importance because too small an angle would lead ultimately to almost no radiation from the antenna. Clearly though Θ is dependent upon the mast height available and on L_1.

Measurements of Z_3 were made using the antenna where L_1 = 27,51 m, L_2 = 12,2 m; and Z_2 = 400Ω. Its performance in a horizontal configuration at a height of 12m was shown in Fig. 6.12. The effect of changes in Θ on the frequency at which the minimum VSWR occurred was noted and the results are shown in Fig. 6.15 for the case of the 24 MHz band. As Θ is decreased so the frequency at which the lowest VSWR occurs also decreases. The ordinate of Fig. 6.15 is Δf, the difference between the optimum frequency when the antenna was horizontal (Θ = 180°) and that corresponding to the apex angle in question.

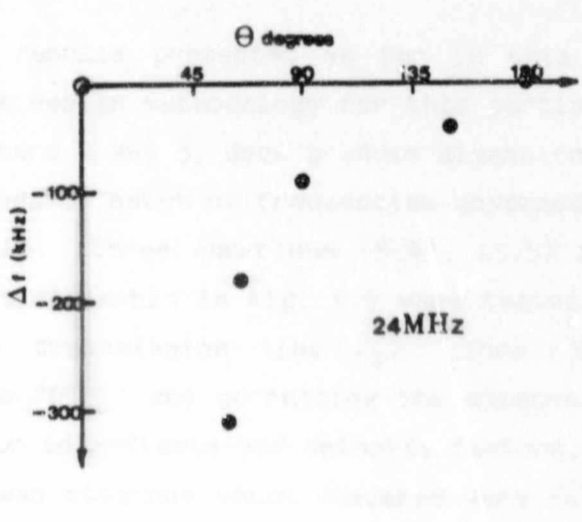

Figure 6.15 : The change in the optimum matching frequency as a function of the apex angle of the inverted vee antenna

Because of the particular antenna length and mast height involved here the smallest apex angle possible was fractionally less than 60°. At that angle the ends of the antenna were just clear of the ground. The rapid increase in Δf as Θ approaches 60°, compared with the change at larger angles, is indicative of the increased capacitive coupling between the ends of the antenna and ground. At frequencies lower than 24 MHz the effect was more diffucit to measure accurately. However at 7 MHz, for example, the change in optimum frequency from $\Theta = 90°$ to $\Theta = 60°$ was about 50 kHz as opposed to the more than 200 kHz at 24 MHz.

While the single mast configuration offers the advantage of simplicity without markedly altering the impedance match, as long as $\Theta \geq 90°$, it also will introduce a vertical component into the radiation pattern of the antenna. In a tactical situation this additional polarization component can be most useful because it allows for groundwave propagation as well as the skywave component with a polar diagram which is almost omnidirectional in azimuth (Jones, 1976) for $\Theta = 90°$.

6.2 The Optimised Design Equations For This Multiband Wire Antenna

The experimental results presented so far in this chapter have confirmed that the design methodology for this particular antenna, developed in chapters 4 and 5, does produce dimensions which yield an acceptable impedance match on frequencies governed by an almost linear relationship. Three equations (5.4), (5.5) and (5.6) and their graphical relationship in Fig. 5.9 were tested by measuring the VSWR on the transmission line Z_4. Then, by using the analytical program "G5RV" and correcting the antenna and matching section lengths for end-effects and velocity factors, a "best-fit" predicted result was obtained which compared very favourably with those measured (see Fig. 6.14). The characteristic impedance, Z_2, of the matching section was the variable in this curve-fitting procedure and the best match occurred with Z_2 nominally 360Ω. The particular transmission line, when measured, was found to have $Z_2 = 355\Omega$.

From these optimised values of L_1, L_2 and Z_2 we are now able to adjust (5.4), (5.5) and (5.6), either by correcting the slopes of (5.4) and (5.5) or by correcting their points of intercept with their respective ordinates. These operations are carried out in Appendix K, from which we obtain:

$$L_1 f_{min} = 359,19 - 1,631 L_2 f_{min} \quad (6.4)$$

or

$$L_1 f_{min} = 482,72 - 2,95 L_2 f_{min} \quad (6.5)$$

which follow from the fact that over the range $Z_2 = 350\Omega$ to $Z_2 = 400\Omega$ the antenna system would match effectively, regardless of Z_2 itself. This is evident from Fig. 5.3. Thus, by eliminating Z_2 from the equations which define how $L_1 f_{min}$ and $L_2 f_{min}$ relate to it and solving simultaneously we arrive at (6.4) and (6.5). Equating these two then yields the following:

$$L_1 f_{min} = 206,44 \quad (6.6)$$

and

$$L_2 f_{min} = 93,65 \quad (6.7)$$

From (6.6) and (6.7) we then use the program "G5RV" to determine the relationships between the frequencies, f_N, on which matching occurs. Appendix K shows this series to be:

$$f_N = 1 : 1,99 : 2,53 : 3,49 : 4,07 : 5,62 : 7,18 : ..... \quad (6.8)$$

It should be noted that the lengths L_1 and L_2 in (6.6) and (6.7) are electrical lengths which must be reduced in practice. Typically a reduction of L_1 by 3 per cent was shown to produce excellent agreement between predicted and measured results. In practice therefore this optimised, thin-wire antenna would be cut to length $L_{1(phys)}$ where,

$$L_{1(phys)} = 200/f_{min} \quad (6.9)$$

Similarly $L_{2(phys)} = L_2 \times$ Velocity Factor

Typically this Velocity Factor for solid dielectric parallel conductor transmission line is quoted as 0,80 to 0,85. For the particular line used in this experimental work it was measured (Appendix J) and found to be 0,81. In general, to cater for the spread,

$$L_{2(phys)} = (74{,}9 \text{ to } 79{,}6)/f_{min} \qquad (6.10)$$

depending on the velocity factor of the specific transmission line used.

6.3 Conclusion

The design equations and analytical techniques developed in Chapters 4 and 5 were tested and shown to yield reasonable results. After comparison of the predicted and measured data the critical dimension of the antenna, L_1, was increased slightly with most promising results. By fitting the predicted results to their optimised practical geometry the corrected design equations were obtained and in view of the fairly non-critical nature of Z_2 (between two defined limits) it was possible to formulate two remarkably simple relationships between L_1, L_2 and the lowest frequency of operation, f_{min}.

The frequencies on which the antenna yields a better than 2:1 impedance match to the transmission line Z_4 were found to be almost linearly related and compared very favourably with those established analytically in Chapter 5.

The effects of the height of the antenna above ground and other objects was also examined. An anomalous matching condition at a frequency approximately $f_{min}/2$ was examined closely and it was postulated that ground losses, with a concomitant decrease in radiation efficiency, were the cause of this. Finally the effect of using only a single mast to support the antenna at its apex was examined experimentally. It was shown that for an apex angle greater than 90° the effect on the impedance match was to decrease slowly the frequency at which the optimum match occurred. For smaller angles the change was very rapid. This effect is considerably more marked at the higher frequencies where the antenna supports a number of current standing waves.

7 DISCUSSION AND CONCLUSIONS

A high-frequency, multiband antenna system for use in tactical and other similar point-to-point radio communication applications has been analyzed and a design methodology developed and tested. The concept of a multiband antenna as opposed to a broadband antenna was examined critically in terms of the operational requirements imposed by the ionosphere and the physical limitations set by size and ease of deployment.

The analytical procedure developed here made extensive use of the Smith Chart and introduced the concepts of a Target Area and a Zone of Possible Matching, both of which enabled a full understanding of the antenna's characteristics to be obtained. A logical consequence of this graphical analytical approach was the development of a computer-based method of analysis. Fundamental to both approaches was the availability of suitable driving-point impedance data from which to commence the analysis. Whereas the modern approach is to obtain these data by solving a set of defining integro-differential equations (usually by the Method of Moments), in this work data already available in the literature was used. These data were in a form which made them directly applicable to this work and their accuracy was beyond doubt in that they are used frequently as the "standard" against which various results obtained from other approaches, such as the Method of Moments, are judged.

A computer program, using these driving-point impedances, enabled the various inter-relationships which exist between the antenna's system components to be determined. From these a design methodology was developed.

The sophistication of modern communications electronics has made possible radio equipment with considerable frequency flexibility and agility. Unfortunately its use has, in many cases, not been coupled with an appreciation that the most significant factor limiting its performance is the environment in which it is operating. At HF the most crucial component of this multi-faceted environment is the Ionosphere. In this work the characteristics of ionospheric propagation were examined in so far as they affect relatively short-range ($\leq$ 1 200 km) paths. It is well known that effective communications over a 24 hour period, via an ionospheric path, require a number of changes in frequency to be made, typically to cater for the marked changes in the ionosphere between midday and midnight. In essence three frequencies could probably suffice: one each for the daytime and nightime paths and another to cover the sunrise-sunset transitions. By analysing available propagation-prediction data for single-hop, temperate and equatorial paths, for a period of more than an 11-year sunspot cycle, it was shown that three different cyclical phenomena existed if the ratio of the noon FOT to the midnight FOT were plotted against the months in question. Of particular interest was the fact that the graphs at 0° and 30° latitudes displayed dissimilar growth or decay characteristics. However that result in itself was not of primary importance in this work, rather it was the change in peak-to-peak amplitude of the curves, over a period of time.

Whereas at a peak in sunspot count at 30°S, frequencies in the ratio of five or more would be required to cover the path, a range of only two to three would be necessary during sunspot minima. By contrast, at the equator, a ratio of less than two-to-one would suffice at periods of high solar activity rising to around two-to-one during the minima.

This result which appears not to have been reported previously is significant because it implies that frequency allocation and particularly the type of antennas required would differ markedly, both with season and locality. Whereas an antenna covering only an octave of frequency would suffice at the equator, one with considerably greater bandwidth is required in the southern temperate zones. However it was shown that an antenna which has the capability of operating effectively on discrete bands of frequencies, which extend over a range of five or more would be as effective. In fact it could be even more effective if its more restricted frequency coverage is compensated by greater radiation efficiency and possibly by less bulk. The antenna system discussed in this work was shown to be a prime candidate for consideration.

Up to eight bands of HF frequencies, related by a defined series, could be covered by a single antenna. When the locality and sunspot conditions make it necessary to use frequencies in the ratio of five, or six to one, to provide 24 hour coverage over a particular path then this multiband antenna system provides that flexibility in a particularly simple structural configuration without sacrificing efficiency. The more conventional approaches used to solve this antenna problem frequently involve broadband structures whose bulk and complexity make them completely unsuitable for rapid, easy and inconspicuous deployment. By contrast, considerably smaller antenna systems, which of necessity must include some additional hardware to compensate and correct for the intrinsically narrowband nature of electrically small antennas, are inherently inefficient radiators.

Whereas the analytical and design processes in this work considered the antenna system to be in freespace it was of course most necessary to examine its performance in realistic situations. Of these, the fact that the antenna could never be overly high (particularly in its tactical role) is the most important. Numerous measurements were made with the antenna height as the parameter. It was found that the freespace impedance data used in the analysis were entirely adequate for design purposes in general. Coupling between the antenna and its image in the ground produced an additional, acceptable impedance match below the predicted low-frequency limit. Investigation showed this to be the case over a very narrow bandwidth though and calculations indicated that the radiation efficiency of the antenna was very low, due to increased losses in the ground. Further impedance measurements, at heights less than 0,1λ above the ground, enabled values of conductivity and relative permittivity for the particular soil beneath the antenna to be derived from published results. While it was not the intention to use this antenna as a geological probe the values obtained agreed reasonably well with those in the literature for similar geographical areas and thus provided a degree of confidence in the measurement procedure which was used.

Similarly the effect of changing the geometry of the antenna from that of a horizontal radiator to an inverted vee configuration was examined experimentally. The effect on the impedance match and, by inference, on the driving-point impedance was dependent upon both the apex angle of the antenna and on the excitation frequency. At the high frequency end of the HF band the change in impedance with decreasing apex angle was much more rapid than nearer 3 MHz. It was shown that 90° was probably the minimum value of included angle that should be used in practice. That result was useful, if not all that novel, simply because it set a practical limit on minimum mast height, given a defined low frequency limit.

Comparison of the measured and predicted performance of the antenna system finally meant that two very simple design equations could be formulated. The first set the length of the antenna, given the lowest frequency on which operation was required and the second enabled the length of the series-section matching transformer to be calculated.

The antenna itself falls into the class of "thin-wire" structures. The actual physical length of the antenna conductor is less than its electrical length by an amount which allows for the inherent end-loading caused by any mounting and support hardware. If, as would be the case in tactical situations, the silhouette is to be as insignificant as possible, then any end-loading would, per force, be minimal.

The series-section transmission line transformer was shown analytically and confirmed experimentally, to be the key element in determining the performance of the antenna. The concepts of Target Area (TA) and Zone of Possible Matching (ZPM) were introduced to aid in a graphical analysis of the antenna system.

It was shown that the ideal locus of normalized antenna driving-point impedance on the Smith Chart was a circle centred within the chart. The driving-point impedance itself was a function of the length of the antenna and when normalized with respect to the series section transmission line must fall within the ZPM whose width was that of the TA. This was set by the defined maximum VSWR on the transmission line to the terminal equipment, its characteristic impedance and that of the matching line.

The results described in this work have made possible the design of a simple, antenna system for tactical and certain point-to-point applications. Further areas of research readily suggest themselves. The first of these is a means of replacing the matching line in its present lengthy and somewhat unwieldy form, by a more compact configuration. Another avenue worthy of investigation might be some means of loading the antenna itself so as to change its driving-point impedance, either to reduce its length for the same frequency coverage or to yield even more bands on which matching would occur. Both should be achieved without degrading efficiency or increasing the bulk and cross-sectional dimensions of the antenna.

The research reported here has resulted in a better understanding being obtained of a simple wire antenna configuration which has particular application in tactical situations if maximum performance is to be achieved.

Simple design equations were developed and the effects of the ground on low altitude antennas were examined. It was shown that by paying adequate attention to the prevailing ionospheric conditions and by noting their characteristics both in time and locality, a simple, multiband antenna system could be used most effectively in the field.

APPENDIX A

THE HF BANDS ALLOCATED TO THE AMATEUR SERVICE

The following are the bands of frequencies within the HF spectrum allocated to the amateur service in South Africa. By and large the frequencies shown below are in general use, by radio amateurs, throughout the world. Those differences which do exist are minor and so will not be discussed here.

Frequency Range (MHz)	Radio Amateur Designation (m)
3,5 - 3,8	80
7,0 - 7,1	40
10,1 - 10,15	30
14,0 - 14,35	20
18,068 - 18,168	17
21,0 - 21,45	15
24,89 - 24,99	12
28,0 - 29,7	10

APPENDIX B

THE EFFECT OF LOSSES ON THE CHARACTERISTIC IMPEDANCE OF COAXIAL CABLE

The characteristic impedance of coaxial transmission line is given by

$$Z_o = \sqrt{(R+j\omega L)/(G+j\omega C)} = (138/\sqrt{\varepsilon_r})(\log D/d)$$

where R,L,G and C are the per unit values of the cable "constants";

ε_r is the relative permittivity of the dielectric and D and d are the diameters of the adjacent surfaces of the coaxial conductors.

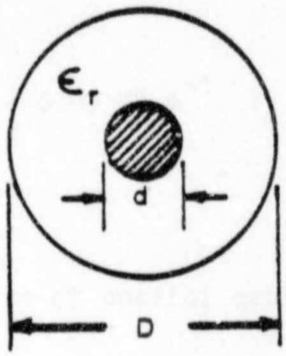

Figure B.1 : The cross-section of a coaxial cable

Now line losses are related to the propagation factor of the line, γ, where

$$\gamma = \sqrt{(R+j\omega L)(G+j\omega C)} = \alpha + j\beta$$

after re-arranging and using the binomial expansion we can write

$$\gamma = j\omega\sqrt{LC}\left(1 + \frac{R}{2j\omega L} + \frac{G}{2j\omega C}\right)$$

$$= \frac{R}{2\sqrt{L/C}} + \frac{G\sqrt{L/C}}{2} + j\omega\sqrt{LC}$$

APPENDIX B

THE EFFECT OF LOSSES ON THE CHARACTERISTIC IMPEDANCE OF COAXIAL CABLE

The characteristic impedance of coaxial transmission line is given by

$$Z_o = \sqrt{(R+j\omega L)/(G+j\omega C)} = (138/\sqrt{\varepsilon_r})(\log D/d)$$

where R,L,G and C are the per unit values of the cable "constants";

ε_r is the relative permittivity of the dielectric and D and d are the diameters of the adjacent surfaces of the coaxial conductors.

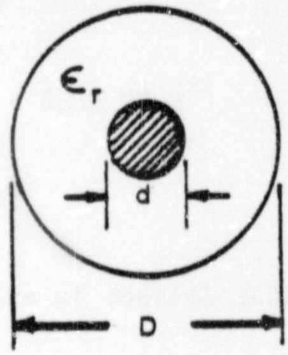

Figure B.1 : The cross-section of a coaxial cable

Now line losses are related to the propagation factor of the line, γ, where

$$\gamma = \sqrt{(R+j\omega L)(G+j\omega C)} = \alpha + j\beta$$

after re-arranging and using the binomial expansion we can write

$$\gamma \approx j\omega\sqrt{LC}\left(1 + \frac{R}{2j\omega L} + \frac{G}{2j\omega C}\right)$$

$$\approx \frac{R}{2\sqrt{L/C}} + \frac{G\sqrt{L/C}}{2} + j\omega\sqrt{LC}$$

thus $\alpha = \frac{1}{2}\left(\frac{R}{Z_o} + G\,Z_o\right)$

where $Z_o = \sqrt{L/C}$ on the assumption that the line is almost lossless.

Now if we ignore dielectric losses (G) in comparison with conductor losses (R) then we write

$$\alpha = R/2\,Z_o$$

or $$R = 2\alpha\,Z_o$$

Using α = 0,08 dBm^{-1} = 0,009 nepers m^{-1} at 30 MHz we have the worst case where

$$R_{30} = 0{,}92\Omega\ m^{-1}$$

while at 3 MHz with α = 0,03 dB m^{-1}

$$R_3 = 0{,}35\Omega\ m^{-1}$$

Now inductance per metre of coaxial cable is (Hall, op cit, p. 3-19)

$$L = 0{,}46 \log D/d\ \ \mu H\ m^{-1}$$

and D/d = 5 for RG58-type (6 mm) coaxial cable therefore

$$L = 0{,}32\ \mu H\ m^{-1}$$

or $$\omega L = 60\Omega m^{-1} \text{ at } 30\text{ MHz}$$

Now low-loss transmission line has

$R \ll \omega L$ (Jordan and Balmain, op cit, p. 218)

and in this case $R/\omega L$ = 0,92/60 = 0,015

and we assumed $G \ll \omega C$

therefore $Z_o = \sqrt{L/C}$ is Real over the range of frequencies of interest here.

APPENDIX C

THE KING-HARRISON DATA FROM WHICH Z_1 WAS OBTAINED (KING AND HARRISON, OP CIT)

IMPEDANCE $Z = R - iX$ (ohms) FOR LONG ANTENNAS IN AIR (WU'S THEORY) WITH $\Omega = 2 \ln (2h/a)$ AS THE PARAMETER

k_0h	$\Omega = 20.0$	$\Omega = 17.5$	$\Omega = 16.0$	$\Omega = 15.0$	$\Omega = 12.5$
1.0	15.24 − 616.02	16.04 − 518.46	16.51 − 459.71	16.78 − 420.43	17.26 −322.03
1.1	25.28 − 480.87	26.01 − 403.47	26.45 − 356.83	26.74 − 325.66	27.40 −247.51
1.2	35.22 − 358.50	36.00 − 299.25	36.53 − 263.53	36.90 − 239.64	37.98 −179.73
1.3	45.79 − 244.64	46.75 − 202.15	47.44 − 176.50	47.98 − 159.33	49.71 −116.21
1.4	57.63 − 136.02	58.89 − 109.36	59.86 − 93.21	60.63 − 82.36	63.33 − 55.06
1.5	71.38 − 29.99	73.09 − 18.57	74.46 − 11.56	75.58 − 6.81	79.64 + 5.27
1.6	87.78 + 75.85	90.15 + 72.27	92.09 + 70.30	93.70 + 69.06	99.73 + 66.19
1.7	107.78 + 183.82	111.10 + 165.18	113.85 + 154.18	116.18 + 146.93	125.04 +128.99
1.8	132.67 + 296.35	137.35 + 262.25	141.30 + 241.98	144.66 + 228.54	157.70 +194.94
1.9	164.27 + 416.19	170.96 + 365.84	176.65 + 335.77	181.54 + 315.76	200.81 +265.20
2.0	205.33 + 546.66	214.97 + 478.69	223.27 + 437.92	230.46 + 410.65	259.18 +340.56
2.1	260.04 + 691.91	274.15 + 604.15	286.39 + 551.13	297.08 + 515.35	340.20 +420.70
2.2	335.16 + 857.30	356.14 + 746.18	374.47 + 678.20	390.54 + 631.64	455.37 +502.23
2.3	442.07 +1049.73	473.82 + 909.12	501.59 + 821.14	525.90 + 759.32	621.53 +573.88
2.4	600.90 +1277.67	649.64 +1096.02	691.82 + 977.94	728.08 + 891.49	858.54 +605.57
2.5	849.24 +1548.97	923.94 +1302.44	985.73 +1132.43	1035.72 +1001.13	1169.83 +531.59
2.6	1260.38 +1859.77	1367.40 +1494.58	1443.21 +1224.81	1491.89 +1008.01	1482.87 +258.75
2.7	1975.18 +2146.23	2077.92 +1541.48	2099.85 +1086.21	2066.77 + 734.57	1607.21 −211.43
2.8	3180.44 +2107.50	3029.63 +1088.67	2754.98 + 433.98	2467.35 + 21.09	1427.64 −658.83
2.9	4641.40 + 930.39	3588.46 − 187.89	2819.39 − 644.48	2289.47 − 831.13	1093.51 −889.47
3.0	4644.77 −1360.38	3021.62 −1485.97	2193.36 −1402.74	1713.63 −1298.45	785.73 −931.28
3.1	3130.00 −2560.76	2024.41 −1938.55	1482.76 −1592.20	1170.97 −1374.50	559.82 −881.26
3.2	1859.31 −2554.50	1285.17 −1860.91	979.32 −1497.59	793.93 −1277.26	405.13 −800.46
3.3	1131.67 −2215.28	835.42 −1637.23	662.28 −1325.39	551.16 −1134.46	300.11 −715.14
3.4	728.05 −1866.46	565.93 −1407.41	463.63 −1152.32	394.64 − 992.52	227.92 −634.51
3.5	493.51 −1570.34	399.10 −1204.71	335.30 − 996.61	291.33 − 864.14	177.47 −560.93
3.6	349.61 −1326.55	291.72 −1031.61	250.97 − 860.83	221.37 − 750.78	141.74 −494.27
3.7	257.23 −1124.18	220.29 − 883.46	193.23 − 742.38	173.01 − 650.61	116.33 −433.58
3.8	195.93 − 952.94	171.67 − 754.92	153.29 − 637.36	139.23 − 561.19	98.43 −377.77
3.9	154.51 − 804.79	138.27 − 641.40	125.61 − 544.21	115.74 − 480.22	86.27 −325.78
4.0	126.48 − 673.79	115.53 − 539.26	106.78 − 458.87	99.85 − 405.75	78.72 −276.68
4.1	107.99 − 555.46	100.67 − 445.62	94.69 − 379.78	89.89 − 336.14	75.12 −229.63
4.2	96.70 − 446.41	91.97 − 358.22	88.04 − 305.23	84.86 − 270.04	75.17 −183.92
4.3	91.19 − 343.97	88.42 − 275.18	86.09 − 233.78	84.20 − 206.25	78.81 −138.89
4.4	90.67 − 245.95	89.50 − 194.94	88.50 − 164.20	87.73 − 143.75	86.27 − 93.96
4.5	94.78 − 150.48	95.04 − 116.11	95.28 − 95.38	95.56 − 81.61	98.08 − 48.60
4.6	103.55 − 55.87	105.26 − 37.41	106.76 − 26.27	108.15 − 18.93	115.09 − 2.38
4.7	117.36 + 39.49	120.68 + 42.41	123.63 + 44.13	126.31 + 45.12	138.58 + 44.98
4.8	136.98 + 137.22	142.28 + 124.57	147.01 + 116.79	151.30 + 111.32	170.45 + 93.46
4.9	163.70 + 239.04	171.57 + 210.37	178.65 + 192.68	185.06 + 180.36	213.35 +142.43
5.0	199.50 + 346.84	210.85 + 301.10	221.11 + 272.65	230.41 + 252.65	270.85 +190.13
5.1	247.40 + 462.74	263.58 + 398.06	278.23 + 357.21	291.47 + 328.02	347.45 +232.52
5.2	312.05 + 589.06	334.98 + 502.20	355.66 + 446.07	374.16 + 404.95	447.76 +261.66
5.3	400.68 + 728.18	432.98 + 613.56	461.65 + 537.02	486.72 + 479.00	573.69 +263.42
5.4	524.77 + 881.81	569.61 + 729.61	607.87 + 623.43	639.52 + 539.79	717.81 +217.22
5.5	702.88 +1049.03	762.56 + 841.43	808.91 + 689.34	842.16 + 565.70	853.98 +103.65
5.6	964.84 +1220.55	1035.20 + 925.30	1076.83 + 700.87	1092.98 + 518.23	937.28 − 74.65
5.7	1355.46 +1363.72	1407.30 + 926.93	1401.30 + 598.72	1355.53 + 347.44	931.1[illegible] −276.42
5.8	1923.96 +1387.60	1857.16 + 747.30	1710.04 + 316.78	1539.09 + 33.42	842.00 −444.18
5.9	2647.00 +1096.16	2245.71 + 287.57	1858.13 − 134.74	1544.56 − 350.96	711.01 −547.17
6.0	3231.65 + 281.59	2330.35 − 378.31	1747.42 − 601.47	1370.45 − 669.82	577.75 −589.89
6.1	3178.17 − 820.65	2039.52 − 953.31	1453.71 − 913.61	1113.89 − 848.24	462.21 −591.57
6.2	2527.19 −1569.17	1583.27 −1244.59	1125.85 −1040.39	865.67 − 903.85	369.23 −569.90
6.3	1794.27 −1794.24	1165.33 −1301.82	848.40 −1043.17	663.30 − 885.33	296.73 −536.57
6.4	1239.47 −1727.72	849.38 −1238.95	638.22 − 984.54	509.54 − 830.89	240.84 −498.27
6.5	866.70 −1560.04	625.48 −1130.51	484.99 − 901.82	395.48 − 762.32	197.82 −458.46
6.6	621.05 −1374.47	468.75 −1011.47	374.04 − 813.07	311.17 − 690.27	164.70 −418.81
6.7	456.89 −1199.07	358.19 − 895.65	293.28 − 725.97	248.58 − 619.45	139.25 −380.04
6.8	344.73 −1040.71	279.22 − 787.50	234.03 − 643.28	201.90 − 551.62	119.85 −342.33
6.9	266.52 − 899.07	222.20 − 687.70	190.35 − 565.56	167.07 − 487.15	105.36 −305.61

$k_0 h$	$\Omega = 20.0$	$\Omega = 17.5$	$\Omega = 16.0$	$\Omega = 15.0$	$\Omega = 12.5$
7.0	211.24 − 771.75	180.84 − 595.45	158.23 − 492.46	141.30 − 425.79	95.03 −269.67
7.1	172.04 − 656.02	151.05 − 509.54	134.97 − 423.25	122.70 − 367.04	88.38 −234.25
7.2	144.59 − 549.37	130.14 − 428.68	118.80 − 357.14	110.01 − 310.31	85.17 −199.05
7.3	126.11 − 449.63	116.36 − 351.63	108.55 − 293.29	102.44 − 254.98	85.39 −163.79
7.4	114.88 − 354.91	108.62 − 277.28	103.55 − 230.93	99.59 − 200.44	89.22 −128.18
7.5	109.83 − 263.61	106.31 − 204.58	103.48 − 169.30	101.34 − 146.11	97.10 − 92.01
7.6	110.43 − 174.25	109.24 − 132.56	108.38 − 107.69	107.90 − 91.43	109.73 − 55.13
7.7	116.56 − 85.49	117.55 − 60.30	118.60 − 45.41	119.78 − 35.88	128.14 − 17.58
7.8	128.51 + 3.96	131.76 + 13.09	134.85 + 18.16	137.86 + 20.99	153.79 + 20.26
7.9	146.98 + 95.39	152.82 + 88.49	158.30 + 83.60	163.48 + 79.49	188.57 + 57.40
8.0	173.20 + 190.14	182.25 + 166.71	190.70 + 151.32	198.60 + 139.67	234.84 + 91.80
8.1	209.08 + 289.68	222.29 + 248.45	234.58 + 221.42	245.95 + 201.03	295.01 +119.63
8.2	257.52 + 395.11	276.24 + 334.09	293.51 + 293.31	309.25 + 262.04	370.57 +134.43
8.3	322.87 + 508.01	348.86 + 423.31	372.40 + 365.09	393.26 + 319.25	459.82 +126.69
8.4	411.66 + 629.05	446.93 + 514.21	477.67 + 432.27	503.35 + 365.74	554.30 + 85.55
8.5	533.75 + 757.55	579.77 + 601.57	616.70 + 485.54	643.72 + 388.94	636.29 + 4.71
8.6	703.90 + 889.13	759.00 + 673.49	795.21 + 507.50	812.53 + 368.92	683.14 −108.69
8.7	943.20 +1010.55	995.31 + 705.76	1009.88 + 470.03	993.02 + 280.99	680.44 −231.74
8.8	1277.39 +1088.90	1287.25 + 655.78	1234.48 + 338.94	1145.58 + 109.81	632.73 −337.59
8.9	1721.67 +1053.75	1596.59 + 467.77	1409.12 + 97.89	1217.35 − 126.48	558.57 −410.76
9.0	2229.89 + 789.58	1825.79 + 114.60	1462.25 − 215.27	1180.39 − 370.43	477.23 −450.47
9.1	2617.37 + 212.17	1859.82 − 333.19	1370.28 − 512.06	1054.71 − 561.43	400.95 −463.98
9.2	2630.92 − 540.50	1680.39 − 724.92	1181.21 − 718.93	889.95 − 674.58	334.89 −459.85
9.3	2257.01 −1138.39	1387.22 − 961.28	965.64 − 821.70	727.11 − 719.58	279.97 −444.91
9.4	1743.42 −1420.70	1089.41 −1048.84	769.24 − 845.66	586.02 − 718.30	235.20 −423.75
9.5	1287.98 −1463.02	839.45 −1040.47	607.99 − 822.07	471.30 − 690.03	199.01 −399.32
9.6	944.84 −1384.75	646.17 − 982.69	481.62 − 773.72	380.64 − 647.65	169.89 −373.19
9.7	700.15 −1260.75	501.24 − 903.73	384.36 − 714.17	309.80 − 598.76	146.56 −346.32
9.8	527.38 −1126.19	393.38 − 818.11	309.87 − 650.67	254.62 − 547.44	127.98 −319.17
9.9	404.50 − 995.19	312.93 − 732.58	252.83 − 586.80	211.72 − 495.80	113.41 −291.94
10.0	316.10 − 872.39	252.71 − 649.87	209.16 − 524.13	178.48 − 444.74	102.32 −264.66
10.1	251.90 − 756.51	207.58 − 570.80	175.91 − 463.20	153.02 − 394.60	94.34 −237.27
10.2	205.15 − 652.74	174.00 − 495.29	150.98 − 403.99	133.97 − 345.33	89.32 −209.65
10.3	171.37 − 553.79	149.53 − 422.84	132.91 − 346.25	120.42 − 296.72	87.24 −181.66
10.4	147.64 − 460.24	132.50 − 352.80	120.73 − 289.55	111.78 − 248.49	88.24 −153.15
10.5	132.01 − 370.76	121.86 − 284.46	113.86 − 233.45	107.78 − 200.28	92.66 −124.02
10.6	123.29 − 284.08	117.02 − 217.10	112.08 − 177.46	108.41 − 151.72	101.04 − 94.23
10.7	120.82 − 199.02	117.73 − 150.01	115.43 − 121.10	113.94 − 102.48	114.17 − 63.89
10.8	124.39 − 114.49	124.14 − 82.51	124.30 − 63.90	124.92 − 52.26	133.14 − 33.38
10.9	134.16 − 29.39	136.72 − 13.93	139.40 − 5.47	142.25 − 0.84	159.34 − 3.58
11.0	150.77 + 57.34	156.38 + 56.36	161.87 + 54.48	167.27 + 51.77	194.36 + 23.82
11.1	175.33 + 146.76	184.55 + 128.86	193.39 + 116.03	201.85 + 105.20	239.75 + 45.86
11.2	209.59 + 239.90	223.30 + 203.90	236.30 + 178.79	248.45 + 158.41	296.15 + 57.85
11.3	256.20 + 337.72	275.64 + 281.33	293.75 + 241.59	310.22 + 209.14	361.85 + 53.32
11.4	319.05 + 440.89	345.72 + 360.14	369.81 + 301.73	390.68 + 253.07	430.69 + 25.40
11.5	403.84 + 549.35	439.15 + 437.59	469.21 + 353.91	492.82 + 282.59	491.07 − 29.48
11.6	518.81 + 661.39	562.99 + 507.69	596.21 + 388.57	616.80 + 286.23	528.83 −106.76
11.7	675.61 + 771.63	724.75 + 550.59	751.55 + 390.17	755.63 + 248.22	534.52 −192.74
11.8	889.47 + 866.92	928.66 + 569.31	926.33 + 337.70	890.11 + 154.75	509.32 −270.79
11.9	1176.26 + 919.06	[illegible] + 508.11	1094.28 + 211.91	989.00 + 5.04	463.26 −329.68
12.0	1539.79 + 875.12	1403.18 + 341.13	1211.73 + 12.62	1022.16 − 178.18	408.34 −366.65
12.1	1939.50 + 659.08	1570.40 + 61.08	1238.07 − 225.87	981.15 − 355.13	353.48 −384.65
12.2	2251.98 + 221.33	1599.20 − 279.74	1166.52 − 446.81	884.81 − 492.03	303.47 −388.58
12.3	2313.76 − 356.04	1479.21 − 587.12	1028.79 − 607.02	763.57 − [illegible]	260.09 −382.98
12.4	2086.10 − 868.28	1267.97 − 793.80	868.03 − 696.48	641.92 − [illegible]	223.42 −371.26
12.5	1704.13 −1171.92	1036.48 − 892.80	714.71 − 728.26	532.87 − 620.54	192.84 −355.77
12.6	1319.75 −1276.76	827.92 − 912.20	582.47 − 721.28	440.67 − 604.26	167.53 −338.01
12.7	1002.83 −1257.66	656.67 − 883.60	474.00 − 691.22	365.00 − 575.27	146.68 −318.88
12.8	762.16 −1177.86	521.88 − 829.75	387.11 − 648.58	303.78 − 539.20	129.62 −298.93
12.9	584.57 −1074.05	417.56 − 764.25	318.22 − 599.68	254.59 − 499.45	115.81 −278.43

k_0h	Ω = 20.0	Ω = 17.5	Ω = 16.0	Ω = 15.0	Ω = 12.5
13.0	454.15 − 964.19	337.25 − 694.48	263.85 − 548.10	215.25 − 457.96	104.85 −257.52
13.1	357.99 − 856.16	275.48 − 624.12	221.10 − 495.71	183.98 − 415.75	96.47 −236.23
13.2	286.68 − 752.88	228.0[illegible] − 554.85	187.71 − 443.42	159.42 − 373.31	90.54 −214.52
13.3	233.72 − 654.99	191.8[illegible] 487.24	162.02 − 391.54	140.58 − 330.80	87.02 −192.34
13.4	194.60 − 562.13	164.[illegible] − 421.32	142.84 − 340.10	126.76 − 288.20	86.03 −169.59
13.5	166.30 − 473.50	145.26 − 356.80	129.35 − 288.93	117.55 − 245.36	87.80 −146.22
13.6	146.75 − 388.17	132.25 − 293.26	121.08 − 237.77	112.77 − 202.07	92.72 −122.22
13.7	134.65 − 305.17	125.17 − 230.22	117.85 − 186.31	112.50 − 158.12	101.40 [illegible] 97.69
13.8	129.23 − 223.57	123.81 − 167.15	119.76 − 134.21	117.03 − 113.29	114.61 − 72.91
13.9	130.17 − 142.42	128.25 − 103.54	127.17 − 81.17	126.95 − 67.41	133.39 − 48.54
14.0	137.56 − 60.82	138.96 − 38.88	140.81 − 26.94	143.15 − 20.45	158.90 − 25.81
14.1	151.91 + 22.12	156.75 + 27.28	161.75 + 28.58	166.92 + 27.40	192.26 − 6.82
14.2	174.21 + 107.27	182.95 + 95.23	191.57 + 85.24	199.98 + 75.52	234.01 + 5.09
14.3	206.04 + 195.44	219.46 + 165.06	232.38 + 142.40	244.56 + 122.53	283.08 + 5.38
14.4	249.76 + 287.30	268.95 + 236.33	286.95 + 198.53	303.23 + 165.82	335.51 − 10.86
14.5	308.82 + 383.16	335.03 + 307.69	358.63 + 250.65	378.51 + 200.81	383.66 − 46.69
14.6	388.13 + 482.54	422.34 + 376.12	450.86 + 293.31	471.75 + 220.21	417.68 −100.09
14.7	494.61 + 583.38	536.31 + 435.62	565.93 + 317.53	580.84 + 213.73	429.91 −162.80
14.8	637.60 + 680.25	681.92 + 475.33	702.08 + 310.06	696.96 + 169.77	419.15 −223.40
14.9	828.56 + 761.30	860.28 + 477.59	848.90 + 255.15	802.15 + 80.88	390.75 −272.73
15.0	1078.20 + 803.07	1061.66 + 418.18	983.22 + 141.46	872.59 − 48.15	352.78 −306.99
15.1	1386.63 + 764.90	1256.40 + 274.35	1072.41 − 26.03	889.74 − 196.49	312.20 −326.84
15.2	1721.87 + 591.96	1394.15 + 44.68	1090.17 − 219.11	852.[illegible]4 − 335.37	273.43 −335.14
15.3	1996.56 + 248.18	1426.73 − 232.19	1034.44 − 397.53	774.78 − 442.94	238.56 −335.06
15.4	2092.08 − 219.47	1344.69 − 490.08	927.68 − 531.40	679.13 − 511.89	208.25 −329.23
15.5	1958.64 − 671.07	1184.35 − 677.48	799.93 − 612.33	581.99 − 546.22	182.38 −319.62
15.6	1670.08 − 982.00	996.51 − 781.83	673.87 − 647.75	492.89 − 554.44	160.53 −307.54
15.7	1342.90 −1128.40	817.39 − 818.30	561.22 − 650.38	415.57 − 544.89	142.19 −293.86
15.8	1050.42 −1153.80	663.18 − 809.29	465.72 − 631.77	350.46 − 523.98	126.89 −279.13
15.9	815.47 −1109.65	537.05 − 773.33	386.94 − 600.36	296.49 − 496.12	114.23 −263.65
16.0	635.14 −1031.63	436.34 − 722.83	322.85 − 561.64	252.14 − 464.14	103.90 −247.61
16.1	498.90 − 939.93	356.78 − 665.22	271.08 − 518.97	215.93 − 429.76	95.70 −231.10
16.2	396.27 − 844.72	294.22 − 604.65	229.52 − 474.30	186.59 − 393.98	89.49 −214.11
16.3	318.81 − 750.59	245.22 − 543.32	196.40 − 428.67	163.09 − 357.33	85.24 −196.63
16.4	260.31 − 659.68	207.12 − 482.23	170.39 − 382.60	144.69 − 320.06	83.01 −178.63
16.5	216.35 − 572.11	177.95 − 421.77	150.49 − 336.28	130.88 − 282.22	82.95 −160.06
16.6	183.82 − 487.73	156.29 − 361.93	136.03 − 289.69	121.34 − 243.76	85.34 −140.91
16.7	160.59 − 405.98	141.19 − 302.51	126.62 − 242.68	115.98 − 204.56	90.61 −121.26
16.8	145.23 − 326.16	132.09 − 243.18	122.12 − 195.07	114.92 − 164.49	99.31 −101.29
16.9	136.89 − 247.51	128.73 − 183.59	122.64 − 146.63	118.49 − 123.41	112.20 − 81.44
17.0	135.16 − 169.25	131.19 − 123.33	128.57 − 97.15	127.26 − 81.[illegible]4	130.14 − 62.55
17.1	140.02 − 90.62	139.88 − 62.03	140.59 − 46.51	142.13 − 38.06	153.99 − 46.05
17.2	151.90 − 10.86	155.57 + 0.63	159.71 + 5.29	164.30 + 5.82	184.28 − 34.21
17.3	171.64 + 70.75	179.44 + 64.83	187.40 + 57.96	195.37 + 49.61	220.58 − 30.21
17.4	200.63 + 154.87	213.24 + 130.48	225.59 + 110.70	237.30 + 91.81	260.59 − 37.71
17.5	240.98 + 241.96	259.33 + 196.99	276.68 + 161.85	292.23 + 129.65	299.41 − 59.52
17.6	295.72 + 332.14	320.86 + 262.88	343.46 + 208.35	361.94 + 158.60	330.13 − 95.45
17.7	369.10 + 424.77	401.73 + 325.12	428.49 + 244.94	446.7[illegible] + 171.86	346.32 −140.90
17.8	466.96 + 517.69	506.21 + 378.02	532.88 + 263.42	543.33 + 160.60	345.31 −188.04
17.9	596.97 + 605.87	637.78 + 411.89	653.70 + 252.55	642.56 + 116.07	329.35 −229.37
18.0	768.13 + 678.93	796.09 + 411.83	780.62 + 200.12	728.53 + 34.47	303.72 −260.56
18.1	988.29 + 717.46	971.69 + 358.65	893.71 + 98.99	782.70 − 77.50	273.88 −280.81
18.2	1256.67 + 689.33	1139.98 + 235.63	967.50 − 44.47	792.75 − 201.76	243.81 −291.55
18.3	1548.80 + 552.37	1261.84 + 42.75	983.04 − 207.18	759.63 − 316.39	215.77 −294.95
18.4	1800.32 + 276.57	1300.23 − 190.89	939.58 − 358.44	695.78 − 405.71	190.75 −293.06
18.5	1919.83 − 112.06	1245.17 − 415.51	853.88 − 475.34	617.11 − 464.60	168.96 −287.52
18.6	1853.54 − 515.23	1120.49 − 588.97	748.51 − 550.34	536.35 − 495.92	150.25 −279.50
18.7	1637.52 − 825.76	964.4[illegible] − 696.06	641.5[illegible] − 587.74	461.00 − 505.80	134.31 −269.82
18.8	1359.68 −1001.48	807.97 − 744.23	543.1[illegible] − 596.62	394.37 − 500.49	120.84 −259.00
18.9	1090.97 −1062.58	667.69 − 749.60	457.65 − 585.92	337.17 − 484.99	109.52 −247.36

k_0h	Ω = 20.0	Ω = 17.5	Ω = 16.0	Ω = 15.0	Ω = 12.5
19.0	863.19 −1048.99	549.13 − 727.40	385.44 − 562.61	288.89 − 462.87	100.11 −235.12
19.1	681.70 − 993.99	451.91 − 668.84	325.46 − 531.49	248.54 − 436.52	92.44 −222.37
19.2	540.88 − 918.85	373.41 − 641.19	276.12 − 495.70	215.06 − 407.46	86.40 −209.17
19.3	432.65 − 835.46	310.50 − 588.82	235.82 − 457.14	187.51 − 376.63	81.92 −195.52
19.4	349.64 − 749.99	260.38 − 534.25	203.17 − 416.93	165.10 − 344.56	79.05 −181.41
19.5	286.05 − 665.33	220.74 − 478.81	177.07 − 375.68	147.26 − 311.53	77.86 −166.81
19.6	237.55 − 582.64	189.83 − 423.13	156.71 − 333.68	133.59 − 277.63	78.54 −151.74
19.7	201.00 − 502.16	166.34 − 367.42	141.50 − 291.01	123.88 − 242.88	81.39 −136.21
19.8	174.21 − 423.68	149.36 − 311.67	131.13 − 247.63	118.07 − 207.19	86.79 −120.36
19.9	155.66 − 346.72	138.36 − 255.67	125.49 − 203.41	116.31 − 170.49	95.26 −104.45
20.0	144.42 − 270.71	133.09 − 199.19	124.71 − 158.21	118.96 − 132.70	107.43 − 89.04
20.1	139.98 − 195.01	133.59 − 141.92	129.17 − 111.89	126.58 − 93.79	123.96 − 75.03
20.2	142.25 − 118.99	140.22 − 83.59	139.30 − 64.40	140.02 − 53.91	145.35 − 63.94
20.3	151.52 − 41.99	153.68 − 23.97	156.68 − 15.81	160.42 − 13.44	171.54 − 57.91
20.4	168.53 + 36.60	175.07 + 37.02	182.05 + 33.50	189.26 + 26.77	201.37 − 59.59
20.5	194.50 + 117.31	205.93 + 99.21	217.36 + 82.66	228.2[illegible] + 65.14	231.91 − 71.42
20.6	231.27 + 200.49	248.41 + 161.94	264.76 + 129.99	279.28 + 98.92	258.51 − 94.23
20.7	281.51 + 286.15	305.24 + 223.71	326.58 + 172.49	343.52 + 123.77	276.06 −125.92
20.8	348.93 + 373.58	379.77 + 281.59	404.81 + 205.21	420.66 + 133.44	281.29 −161.55
20.9	438.51 + 460.73	475.48 + 330.36	499.85 + 220.74	506.94 + 120.33	274.34 −195.26
21.0	556.67 + 543.06	594.92 + 361.43	608.37 + 209.42	593.47 + 77.69	258.23 −222.75
21.1	710.74 + 611.61	737.18 + 362.08	720.67 + 161.42	666.33 + 3.73	237.01 −242.28
21.2	906.91 + 650.24	893.70 + 316.55	819.61 + 71.87	710.63 − 94.42	214.16 −254.16
21.3	1144.55 + 632.97	1044.00 + 211.58	884.47 − 52.93	717.58 − 201.21	191.92 −259.73
21.4	1405.16 + 525.90	1156.52 + 47.05	900.38 − 193.83	688.59 − 299.12	171.50 −260.52
21.5	1640.14 + 302.53	1200.90 − 154.83	866.77 − 326.18	635.15 − 376.03	153.34 −257.89
21.6	1776.74 − 24.81	1166.43 − 354.97	796.54 − 431.22	568.67 − 427.99	137.52 −252.86
21.7	1761.01 − 386.44	1068.75 − 517.53	707.56 − 501.85	499.71 − 457.06	123.87 −246.18
21.8	1604.25 − 691.40	937.47 − 626.02	614.82 − 540.45	434.50 − 467.94	112.20 −238.34
21.9	1370.75 − 888.04	799.40 − 682.78	527.55 − 553.74	375.96 − 46[illegible].53	102.29 −229.68
22.0	1125.80 − 978.68	670.97 − 699.[illegible]	449.98 − 548.87	324.96 − 453.90	93.95 −220.41
22.1	906.64 − 992.21	559.19 − 688.27	383.23 − 531.72	281.30 − 436.01	87.02 −210.66
22.2	725.41 − 958.48	465.34 − 659.66	326.65 − 506.58	244.32 − 413.94	81.42 −200.49
22.3	581.06 − 898.99	388.06 − 620.48	279.74 − 476.31	213.24 − 389.05	77.07 −189.93
22.4	467.95 − 826.92	325.09 − 575.23	240.70 − 442.77	187.33 − 362.18	73.98 −178.99
22.5	379.88 − 749.69	274.15 − 526.61	208.62 − 407.10	166.00 − 333.87	72.20 −167.67
22.6	311.51 − 671.14	233.28 − 476.20	182.60 − 369.98	148.76 − 304.38	71.83 −155.96
22.7	258.67 − 593.12	200.88 − 424.83	161.93 − 331.73	135.33 − 273.84	73.07 −143.88
22.8	218.24 − 516.36	175.77 − 372.88	146.15 − 292.53	125.54 − 242.29	76.17 −131.52
22.9	187.97 − 440.95	157.09 − 320.47	134.96 − 252.37	119.38 − 209.69	81.48 −119.05
23.0	166.28 − 366.67	144.33 − 267.54	128.30 − 211.19	117.02 − 175.98	89.45 −106.78
23.1	152.15 − 293.10	137.22 − 213.91	120.31 − 168.92	118.80 − 141.13	100.54 − 95.31
23.2	144.99 − 219.76	135.80 − 159.38	129.33 − 125.46	125.29 − 105.14	115.16 − 85.57
23.3	144.62 − 146.08	140.38 − 103.74	137.99 − 80.79	137.29 − 68.19	133.46 − 78.98
23.4	151.23 − 71.54	151.59 − 46.84	153.19 − 35.05	155.87 − 30.70	154.91 − 77.34
23.5	165.43 + 4.40	170.41 + 11.34	176.17 + 11.36	182.39 + 6.46	177.93 − 82.56
23.6	188.29 + 82.18	198.27 + 70.59	208.53 + 57.55	218.42 + 41.72	199.62 − 95.83
23.7	221.42 + 162.08	237.07 + 130.23	252.20 + 101.87	265.50 + 72.42	216.27 −116.59
23.8	267.17 + 244.04	289.26 + 188.79	309.19 + 141.47	324.56 + 94.46	224.76 −142.13
23.9	328.78 + 327.36	357.72 + 243.55	381.10 + 171.74	394.88 + 102.15	223.99 −168.34
24.0	410.56 + 410.16	445.39 + 289.75	467.98 + 186.01	472.58 + 88.88	215.21 −191.45
24.1	517.96 + 488.42	554.29 + 319.77	566.44 + 175.82	549.35 + 49.23	201.09 −209.23
24.2	657.16 + 554.46	683.35 + 322.64	667.66 + 132.98	612.95 − 17.48	184.41 −221.20
24.3	833.33 + 594.75	825.11 + 285.02	756.73 + 53.78	651.03 − 104.33	167.28 −227.94
24.4	1046.32 + 587.90	962.39 + 195.72	816.18 − 56.05	656.85 − 197.87	150.98 −230.51
24.5	1282.27 + 505.86	1069.01 + 54.02	833.62 − 180.41	632.42 − 283.56	136.15 −229.95
24.6	1503.97 + 324.58	1119.02 − 123.05	808.16 − 298.7	586.38 − 351.51	123.00 −227.13
24.7	1652.49 + 47.23	1101.03 − 303.96	749.96 − 394.98	529.15 − 398.39	111.52 −222.72
24.8	1675.94 − 277.23	1024.91 − 457.51	673.66 − 462.26	469.17 − 425.73	101.60 −217.19
24.9	1569.04 − 572.78	913.90 − 566.58	592.11 − 501.67	411.77 − 437.25	93.10 −210.85

$k_0 h$	Ω = 20.0	Ω = 17.5	Ω = 16.0	Ω = 15.0	Ω = 12.5
25.0	1376.30 − 783.88	791.40 − 629.93	513.71 − 518.25	359.62 − 436.94	85.83 −203.93
25.1	1155.40 − 899.19	673.37 − 655.55	442.72 − 517.89	313.65 − 428.20	79.80 −196.55
25.2	946.37 − 937.19	567.79 − 653.82	380.63 − 505.64	273.84 − 413.59	74.80 −188.80
25.3	766.80 − 923.51	477.20 − 633.74	327.41 − 485.33	239.74 − 394.90	70.80 −180.73
25.4	619.93 − 879.17	401.26 − 601.99	282.35 − 459.63	210.78 − 373.36	67.78 −172.35
25.5	502.60 − 818.21	338.44 − 563.05	244.54 − 430.34	186.39 − 349.76	65.78 −163.68
25.6	409.87 − 749.10	286.92 − 519.80	213.10 − 398.57	166.08 − 324.58	64.84 −154.71
25.7	336.99 − 676.59	245.03 − 473.96	187.25 − 365.03	149.48 − 298.12	65.08 −145.48
25.8	279.98 − 603.19	211.35 − 426.55	166.42 − 330.11	136.34 − 270.50	66.66 −136.02
25.9	235.78 − 530.06	184.79 − 378.08	150.18 − 293.99	126.55 − 241.76	69.81 −126.44

APPENDIX D

CHARACTERISTICS OF THE SMITH CHART IN ITS OFF-CENTRE CONFIGURATION

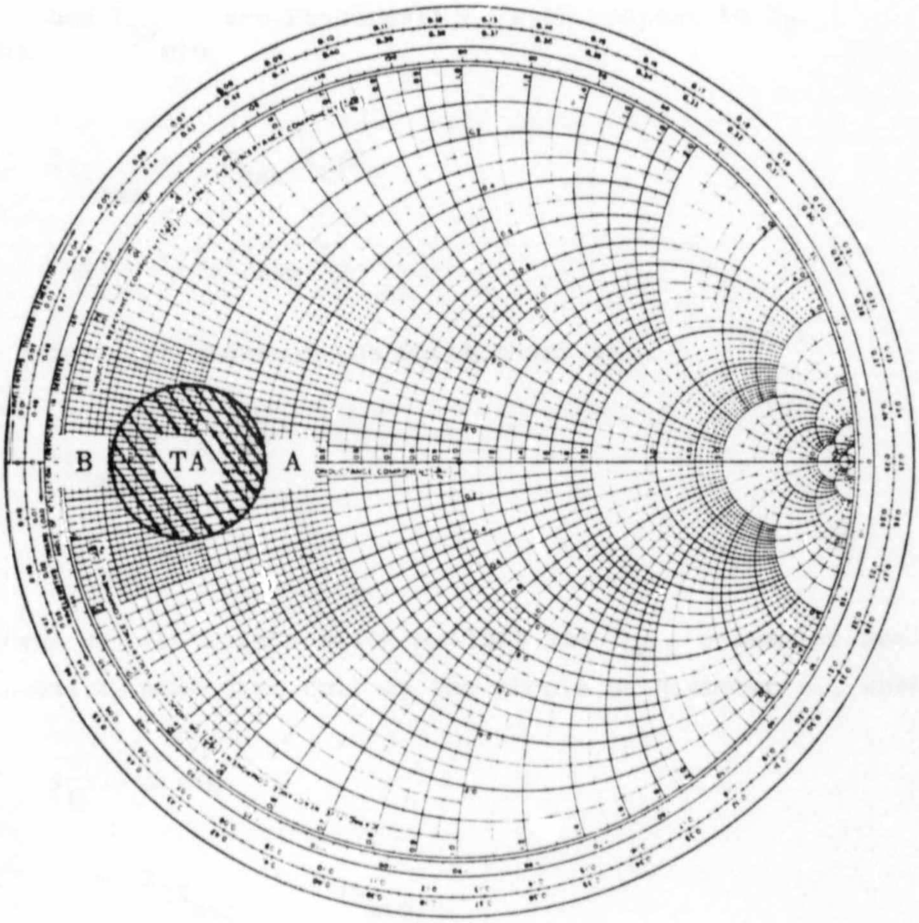

Figure D.1 : The Smith Chart showing the Target Area

If the maximum VSWR on Z_4 is S_{max} then the limits of the Target Area (TA) on the real axis are set by the maximum and minimum values of Z_3 normalised with respect to Z_4.

Thus $$Z_{3_{max}}/Z_4 = S_{max}$$

$$Z_{3_{min}}/Z_4 = 1/S_{max} \quad : \quad S \geq 1 \text{ by definition}$$

Now these values must be related to the driving-point impedance, Z_1, of the antenna, which implies that both must now be normalized again, this time with respect to Z_2 and by so doing the Smith chart exhibits an "off-centre" characteristic when $Z_{3N_{max}}$ and $Z_{3N_{min}}$ are re-normalized with respect to Z_2.

Thus $Z_{3N_{max}} = S_{max} Z_4/Z_2$

while $Z_{3N_{min}} = Z_4/S_{max} Z_2$

These points are shown on the Smith chart by

$Z_{3N_{max}}$ as A

and $Z_{3N_{min}}$ as B

The locus of all points which satisfy the S_{max} criterion for Z_1, Z_2, Z_3 and Z_4 must then fall on the circle of diameter d_1, where

$$d_1 = A - B$$

$$= Z_{3N_{max}} - Z_{3N_{min}}$$

$$= S_{max} Z_4/Z_2 - Z_4/S_{max} Z_2$$

i.e. $d_1 = (Z_4/Z_2)\left((S^2_{max} - 1)/S_{max}\right)$